Magnetization reversal by confined droplet growth in soft/hard hybrid nanodisks with perpendicular anisotropy

J.-P. Adam,[1,*] S. Rohart,[1] J.-P. Jamet,[1] J. Ferré,[1] A. Mougin,[1] R. Weil,[1] H. Bernas,[2] and G. Faini[3]

[1]*Laboratoire de Physique des Solides, Univ Paris-Sud, CNRS UMR 8502, F-91405 Orsay cedex, France*[†]

[2]*CSNSM, Univ Paris-Sud, CNRS UMR 8609, F-91405 Orsay cedex, France*

[3]*Laboratoire de Photonique et Nanostructures, CNRS UPR 20, F-91460 Marcoussis, France*

(Received 22 November 2011; revised manuscript received 17 February 2012; published 14 June 2012)

Magnetization reversal dynamics in single perpendicular Pt/Co/Pt high aspect ratio nanodisks have been studied by polar magneto-optical Kerr effect microscopy. The He^+ ion process used to pattern these nanodisks resulted in a soft/hard nanodisk structure. The energy barrier field dependence was determined from the simple exponential variation of the nonswitching probability with time. The standard coherent reversal scenario fails to account for it whereas a two-dimensional-confined droplet model supports the experimental observations. From a ring shaped metastable domain wall in the magnetically soft outer ring, the reversal progresses via the deformation of the domain wall and the expansion of a reversed confined droplet through the nanodisk hard core. This magnetic reversal, governed by domain wall propagation alone, ensures a magnetization reversal reproducibility from nanodisk to nanodisk and the very narrow energy barrier distribution observed.

DOI: 10.1103/PhysRevB.85.214417 PACS number(s): 75.60.Jk, 68.55.Ln, 75.75.Jn

I. INTRODUCTION

Thermal stability of magnetization in nanoelements is widely discussed in therm of KV product (K is the anisotropy constant, V the volume). The underlying hypothesis is that the magnetization reversal occurs through a coherent spin rotation, which is described by the Stoner-Wohlfarth model[1] (energy landscape) and the Néel-Brown theory[2,3] including thermally induced fluctuations. However, micromagnetics theory, which describes noncolinear magnetization states, shows that such a reversal is limited to dimensions below the domain wall width (a few nanometers in high anisotropy materials) or exchange length (5–10 nm).[4,5] The lowering of the switching field in larger elements, known as the *Brown's paradox*, has been widely debated and all models show the major role played by defects (hard/soft anisotropy inclusions,[6] surface anisotropy,[7] and inhomogeneous demagnetizing field).[8] At a finite temperature, few models are going beyond the Néel-Brown picture.[9,10] The simplest to use invoke a nucleation and propagation of a reversed domain and show that the stability criterion should be expressed in terms of domain wall energy and particle section.[10–12]

In order to master reversal magnetization and obtain homogeneous reversal properties in an assembly of nanoelements, the nucleation of domain wall needs to be precisely controlled by intrinsic parameters. Nanoelements made from perpendicularly magnetized ultrathin films display generally broad variations in switching fields since reversal is controlled by nonuniform nucleation over the pristine film granular structure.[13–15] In this paper, we study nanodisks with a hard magnetic core surrounded by a soft magnetic ring, designed by He^+ irradiation. Although coherent reversal is impossible due to the lateral dimension, a Néel-Brown-like law is still measured in single particles, which indicates that reversal occurs with a single and precisely defined mechanism, with rather uniform properties among the assembly. Extending nucleation and propagation models to this situation, we show that the spontaneous nucleation of an annular shaped domain in the soft ring is at the origin of the homogeneous properties, without reducing the magnetization thermal stability of the nanostructures.

II. SAMPLE PREPARATION

An array of 130-nm-diameter, $2R_e$, magnetic nanodisks [see inset, Fig. 1(b)] was obtained by patterning a sputter-grown, (111) textured, Pt(3.5 nm)/Co(d = 0.5 nm)/Pt(4.5 nm)/Al_2O_3 ultrathin film exhibiting uniaxial magnetic anisotropy perpendicular to the sample plane. We realized magnetic patterning[16] of this film by He^+ ion irradiation through a specially designed mask. Lying on the pristine film, an array of SU-8 resist nanopillars, covered by Ti, was first patterned by electron beam lithography and reactive ion etching. The film was then irradiated by 30 keV He^+ ions at a fluence ($F = 3 \times 10^{16}$ He^+ ions cm^{-2}) such that the unprotected film area became paramagnetic.[16,17] The magnetic properties of the Pt/Co/Pt film, such as the saturation magnetization M_s, the exchange stiffness A, the effective uniaxial anisotropy K, defined as the sum of the demagnetizing anisotropy and of the uniaxial anisotropy due to both the volume and surface anisotropies, and the Curie temperature T_C are all tuned by the He^+ ion irradiation that intermixes Co and Pt ions at the interfaces in a controlled way. Unlike the usual irradiation based on Ar^+ ions, or even heavier ions, irradiation with He^+ ions leads to a soft modification of the thin film structure and of the magnetic properties. Therefore rather than inducing strong defects, He^+ irradiation allows a soft and controlled modification of the magnetic properties with a more homogeneous magnetic thin film as evidenced by the domain wall motion[18] or a soft patterning of the magnetic media as we report here.

The light He^+ ions penetrated into the substrate well below the film and produced essentially no surface erosion, but the SU-8 thickness was insufficient to avoid some irradiation of the film under the nanopillars. The irradiation fluence dependencies of M_s, A, and K were determined from superconducting quantum interference device (SQUID) and magneto-optical

TABLE I. Values of the micromagnetic parameters and of the quality factor of the Bloch domain wall at the fluence $F_{hc} = 4 \times 10^{15}$ He^+ cm^{-2} estimated inside the nanodisk hardcore.

Fluence (He^+ cm^{-2})	A_{hc} ($J\,m^{-1}$)	K_{hc} ($J\,m^{-3}$)	$M_{s_{hc}}$ ($kA\,m^{-1}$)	Q_{hc}	Δ_{hc} (nm)
4×10^{15}	10^{-11}	1.2×10^5	1050	1.2	9

magnetometry measurements on reference unpatterned films, irradiated uniformly. Comparing their magnetic properties, a residual fluence F_{hc} estimated to be 4×10^{15} He^+ ions cm^{-2} has reached the nanodisk hard core, leading to the modification of the micromagnetic properties in the nanodisk hard core, $M_{s_{hc}}$, A_{hc}, and K_{hc}. Their values are summarized in Table I as well as the quality factor $Q = \frac{2K}{\mu_0 M_s^2} + 1$ and the domain wall width $\Delta = \sqrt{\frac{A}{K}}$ at F_{hc}. Next, the radial dependence of nanodisk magnetic properties was deduced from the mask edge-induced fluence variation. Crucial to our purpose is that, due to a well-understood and modeled differential ion scattering effect near the mask edge [see inset in Fig. 1(a)], the irradiation produces nanodisks composed of a magnetically hard core surrounded by a soft ring.[19,20] The magnetically hard core diameter of the nanodisk, irradiated with F_{hc}, was estimated to be $2R_{hc} = 80$ nm, and the fluence increases linearly to its nominal value F at the outer edge of the 25-nm-wide magnetically softer ring. As plotted in Fig. 1(a), M_s is constant in the hard core but decreases exponentially through the ring to cancel in the paramagnetic surrounding region irradiated at the fluence F. This nonuniformity also affects the anisotropy and exchange constants [not shown in Fig. 1(a)]: the magnetic anisotropy and exchange constant varied quadratically with M_s whereas the latter decreased exponentially with fluence.

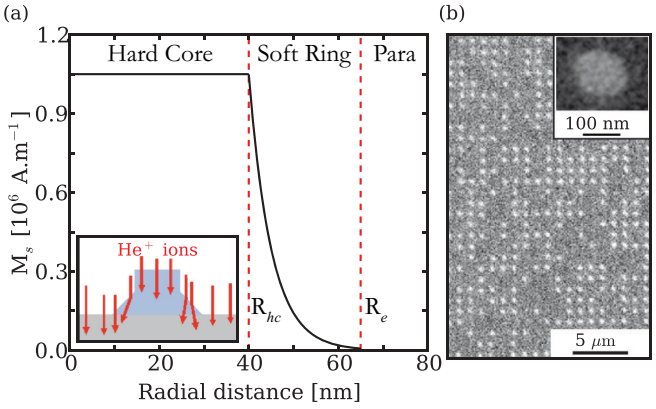

FIG. 1. (Color online) (a) Expected spontaneous magnetization M_s variation along the nanodisk radius. The inset is a schematic representation of the lateral He^+ irradiation under the edge of the SU-8/Ti nanopillars. (b) PMOKE image difference between the remnant state after a magnetic field pulse (27 mT, 200 ns) and the remnant state after saturation under 500 mT during 5 s. White contrast corresponds to nanodisks with reversed magnetization states; nonreversed nanodisks (in gray) cannot be distinguished from the surrounding paramagnetic region. The inset is a magnified SEM image of one 130-nm nanodisk obtained after He^+ irradiation through the SU-8/Ti pillar mask and its subsequent removal.

III. MAGNETO-OPTICAL MICROSCOPY ON INDIVIDUAL NANODISKS

After mask removal, a planar magnetically patterned film can be studied optically. The room temperature remnant magnetization state of 96 nanodisks, obtained after saturating the sample and applying a reversed field H, was probed by high spatial resolution polar magneto-optical Kerr (PMOKE) microscopy at the 510 nm wavelength. As shown on a typical PMOKE image [Fig. 1(b)], the up or down magnetic states of each nanodisk can be probed individually since their separation (1 μm) far exceeds the PMOKE microscope resolution (300 nm). Moreover, since the separation between nanodisks is much larger than their diameter and the magnetic layer is very thin ($d = 0.5$ nm), the exchange and dipolar interdisk couplings are not relevant. This allows studies of isolated nanodisk behavior as well as that of a nanodisk assembly in a single experiment.

For thermally activated transitions between two states, the nonswitching probability law $P(\delta t)$ as a function of the field pulse duration δt depends on diverse processes and activation energies. For a unique checked mechanism, a single energy barrier ΔE is probed, and $P(\delta t) = \exp(-\delta t/\tau)$ with a switching time τ given by the Arrhenius law $\tau = \tau_0 \exp(\Delta E/k_B T)$, τ_0 being the characteristic time of the transition mechanism. Such simple behavior was only reported in rare model systems.[11,21] In most cases, several mechanisms compete and imply a combination of sequential thermally activated mechanisms leading to a nonexponential probability law.[13,22,23]

We have determined this probability law versus the pulse duration at a fixed magnetic field of 24.2 mT applied during δt [shown for four selected nanodisks in Fig. 2(a)]. For each of the 96 nanodisks, $P(\delta t)$ was adjustable to an exponential law demonstrating that in this case the mechanism was unique,[22]

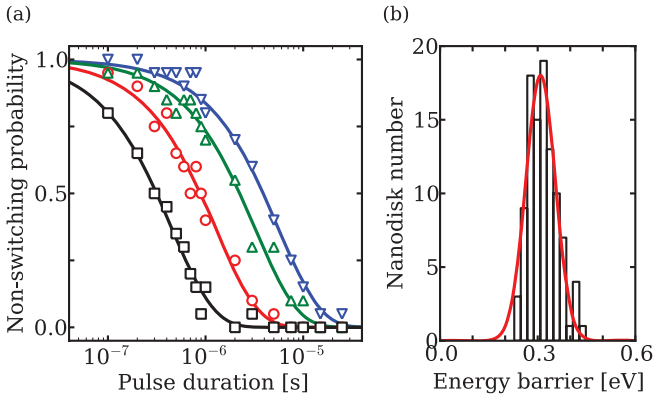

FIG. 2. (Color online) Examples of the nonswitching probability $P(\delta t)$ variation measured on individual nanodisks, under magnetic field pulses of 24.2 mT lasting from 100 ns to 25 μs. The reversal time τ, for which $P(\delta t = \tau) = 1/e$, is determined by fitting the experimental $P(\delta t)$ curve with a single exponential. (b) The energy barrier distribution, assuming $\tau_0 = 10^{-11}$ s in the Arrhenius law, is a Gaussian centered on 0.31 eV with a narrow FWHM = 0.09 eV.

and the characteristic reversal time was determined. Assuming $\tau_0 = 10^{-11}$ s,[24] the energy barrier ΔE for each nanodisk was estimated. Our resulting ΔE distribution is a narrow Gaussian [Fig. 2(b)], proving the magnetization reversal mechanism uniformity over the nanodisk array.

The study was extended to different field amplitudes. For a given pulse duration, the switching field distribution over the whole assembly is again Gaussian with a narrow full width at half maximum (FWHM) [see Fig. 3(a)]. The switching field H_{SW} versus the pulse duration was determined and is reported in Fig. 3(b). As expected, the shorter the pulse duration, the larger the switching field. Nevertheless, it only varies by a factor of 3 for pulse durations differing by eight orders of magnitude. More insight into magnetization reversal dynamics is obtained by considering each nanodisk individually. They all present the same typical H_{SW} variation with δt. Normalizing the pulse duration to the switching time found at 24.2 mT, all the data merge onto the same master curve attesting to a unique reversal mechanism for the entire assembly [inset of Fig. 3(b)]. The energy barrier $\Delta E(H)$ was also estimated as described previously for each nanodisk and is plotted in Fig. 4 for the same nanodisks as in Figs. 2(a) and 3(b). ΔE decreases with the magnetic field and is lower than 0.8 eV for the studied magnetic field range.

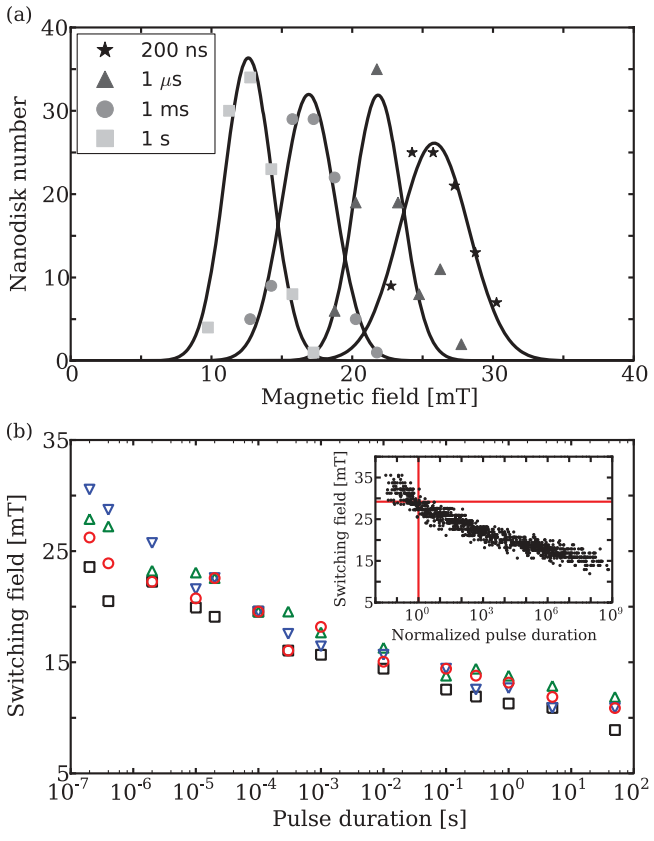

FIG. 3. (Color online) (a) Nanodisk switching-field distributions for four pulse durations: 200 ns, 1 μs, 1 ms, and 1 s. Mean values and FWHM are (25.8 mT, 5.8 mT), (21.8 mT, 4.0 mT), (16.9 mT, 4.4 mT), and (12.6 mT, 4.0 mT), respectively. (b) Switching field H_{SW} variation versus the pulse duration for the nanodisks considered in Fig. 2(a). Inset: data for all the nanodisks, presented for a pulse duration normalized to the switching time determined at $\mu_0 H = 24.2$ mT.

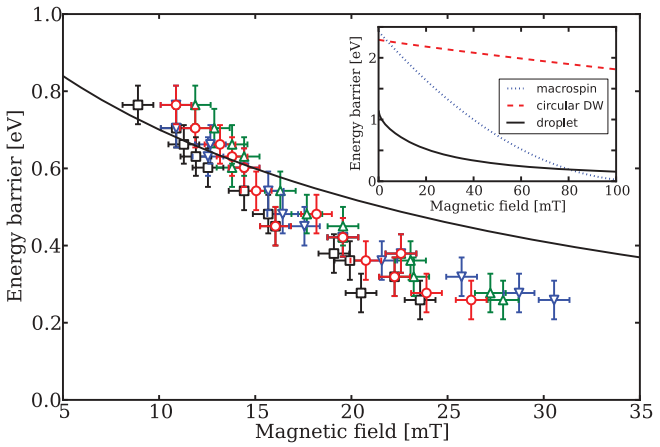

FIG. 4. (Color online) Variation of the energy barrier $\Delta E(H)$ with the field for the nanodisks presented in Fig. 2(a) (open dots) and comparison with our analytical confined droplet model (continuous line). The inset represents the field dependent calculated curves for different mechanisms: the macrospin Stoner-Wohlfarth reversal (dotted line), the circular domain wall (DW) shrinking (dashed line), and the confined droplet growth (continuous line). A crossover between the coherent and confined droplet behaviors is observed around 85 mT.

IV. DISCUSSION AND MODEL

Two archetypal mechanisms are usually suggested to explain the magnetization reversal: coherent magnetization reversal for small nanoparticles, or random domain nucleation followed by domain wall propagation in larger nanoelements.

The rather large nanodisk diameter, as compared to the exchange length ($\Lambda = 3.7$ nm) and domain wall width ($\Delta = 9$ nm), rules out coherent reversal. This is confirmed by calculating the energy barrier ΔE_{S-W} associated to the Stoner-Wolharth mechanism (see dotted line in Fig. 4 inset), and comparing it to the experimental values. For a typical field of 20 mT, ΔE_{S-W} is about 1.6 eV, which is more than four times higher than the experimental results. The reversed domain would be much smaller than the nanodisk volume. A second process, would then be required, resulting in a nonsingle exponential nonswitching probability law. The usual mechanism involving such a random nucleation followed by domain wall propagation generally leads to large switching field distributions, essentially because intrinsic and/or extrinsic defects induce randomness in nucleation fields, and thus a spread in switching field distributions.[13,25]

In the following we show that the gradient in the nanodisk ring plays a major role in the domain wall nucleation and thus provides a narrower switching field distribution.

In our nanodisk, as compared to similar nanoelements obtained by physical etching or lift-off methods,[26] the main difference comes from the gradient of the magnetic properties in the outer ring as depicted in Fig. 1(a). Since both A and K are quadratic with M_s, the domain wall energy density σ_W is also exponentially decreasing in the irradiated ring. The domain wall energy therefore vanishes at the nanodisk border and increases in the ring, reaching $\sigma_{W_{hc}} = 4\sqrt{A_{hc}K_{hc}}$ inside the core, mirroring the nanodisk radial symmetry.

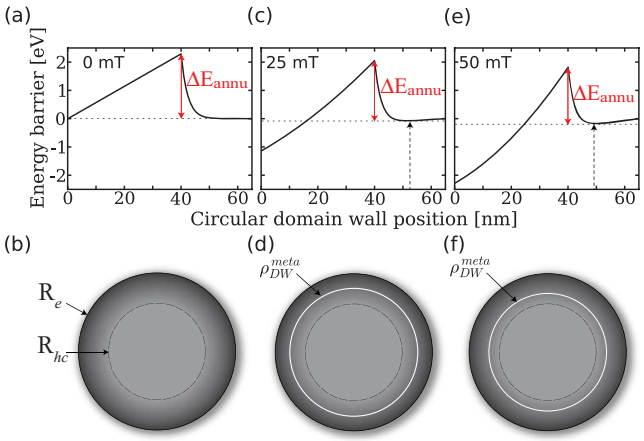

FIG. 5. (Color online) (a), (c), and (e) Energy profiles as a function of the radial position of a circular domain wall obtained from an analytical 2D-Ising model for different values of the applied magnetic field (0 mT, 25 mT, and 50 mT, respectively). The energy origin is the energy of the saturated nanodisk with a magnetization antiparallel to the applied magnetic field. The vertical arrows represent the local micromagnetic energy minima, where the domain wall is at the metastable position in the soft ring, $\rho_{\mathrm{DW}} = \rho_{\mathrm{DW}}^{\mathrm{meta}}$. (b), (d), and (f) The respective micromagnetic configurations: In a (b) zero applied magnetic field, no circular domain wall is stabilized inside the nanodisk; under (d) 25 mT and (f) 50 mT, a circular domain wall occupies a metastable position, the latter being closer to R_{hc} for larger applied magnetic fields.

Taking into account these variations, and assuming the radial symmetry suggested by the magnetic properties of the nanodisk, we developed a simple analytical two-dimensional-Ising (2D-Ising) model, describing the competition between the cost in the circular domain wall energy and the gain in the Zeeman energy in the reversed part. In a zero applied magnetic field, the Zeeman energy gain is zero such that the lower energy configuration is homogeneous. The energy profile exhibits an absolute maximum when the circular domain wall radial position is at $\rho_{\mathrm{DW}} = R_{\mathrm{hc}}$, and two degenerated local minima when the nanodisk magnetization is homogeneously magnetized either with $\rho_{\mathrm{DW}} = 0$ nm or with $\rho_{\mathrm{DW}} = R_e$ [see Figs. 5(a) and 5(b)]. Under a magnetic field antiparallel to the disk magnetization, the Zeeman energy gain increases. For magnetic fields smaller than 3.1 mT, the energy profile differs from the one in a zero applied magnetic field by the lifted degeneracy between the two homogeneously magnetized states: the micromagnetic energy of the configuration parallel to the applied magnetic field ($\rho_{\mathrm{DW}} = 0$ nm) is lower than the antiparallel one ($\rho_{\mathrm{DW}} = R_e$). Above this threshold field, a metastable micromagnetic configuration is predicted with a circular domain wall in the soft outer ring. The configuration with homogeneous magnetization aligned antiparallel to the applied magnetic field is no more stable. The local minima is shifted so that a circular domain wall is expected at $\rho_{\mathrm{DW}}^{\mathrm{meta}}$ in the irradiated outer ring [see Figs. 5(c) and 5(d) for $\mu_0 H = 25$ mT]. The larger the applied magnetic field is, the closer this circular domain wall to the hard core edge [compare the metastable positions indicated in Figs. 5(e) and 5(f) for $\mu_0 H = 50$ mT and in Figs. 5(c) and 5(d) for $\mu_0 H = 25$ mT].

Over the full magnetic field range studied in this experimental work, the energy maximum always takes place at $\rho_{\mathrm{DW}} = R_{\mathrm{hc}}$. There is always an energy barrier to overcome for the wall to penetrate into the hard core part, and the magnetization cannot reverse spontaneously. The predictions of the simple Ising model, which neglects domain wall width, are qualitatively supported by micromagnetic simulations (see Appendix and Fig. 7), which validates this approximation.

We now focus on the magnetization reversal for magnetic fields leading to such a metastable micromagnetic configuration with a circular domain wall in the soft irradiated ring. The remaining question is how the magnetization reverses, i.e., overcomes the energy barrier. The initial configuration rules out coherent magnetization reversal, but also curling or bucking reversals.[5] A straightforward way to reverse the magnetization is to progressively reduce the radius of the circular domain wall, keeping its circular symmetry and thus shrinking the nonreversed core. The saddle point is reached when the domain wall reaches the edge of the hard core. The energy barrier of this mechanism is therefore the difference between the micromagnetic energies for $\rho_{\mathrm{DW}} = R_{\mathrm{hc}}$ and for the metastable configuration with $\rho_{\mathrm{DW}} = \rho_{\mathrm{DW}}^{\mathrm{meta}}$ [see Figs. 5(a)–5(c)]. In the field range experimentally studied, this energy barrier is above 2 eV and higher than the one obtained from a macrospin hypothesis, due to the domain wall length at the saddle point, as shown in the insert of Fig. 4. Such a simple mechanism, while mirroring the symmetry of the nanodisk, is in contradiction with the experimental determination and cannot account for the experimental energy barriers.

From the metastable micromagnetic state, a more efficient mechanism, also involving domain wall motion but breaking the radial symmetry of the nanodisk, corresponds to a local deformation of the metastable circular domain wall. This implies the growth of a confined droplet that propagates in the hard core.[27] Analytically, the droplet can be described by two independent parameters[28] the curvature of the droplet, $\mathcal{C}$, and the penetration of the droplet, $\mathcal{P}$, from its nucleation at $\rho_{\mathrm{DW}}^{\mathrm{meta}}$ (Ref. 29). In order to estimate the associated energy barrier as a function of the magnetic field, we determine the critical value for these two parameters, respectively, $\mathcal{C}_{\mathrm{c}}$ and $\mathcal{P}_{\mathrm{c}}$, at the saddle point. An example of $\mathcal{C}_{\mathrm{c}}$ and $\mathcal{P}_{\mathrm{c}}$ obtained in this way is given in Fig. 6(d) for an applied magnetic field of 25 mT. Their dependence on the applied magnetic field is obtained by the minimizing conditions of the micromagnetic energy of the droplet configuration E_{drop} with respect to both of these parameters. In the 2D-Ising model, one obtains

$$\mathcal{C}_{\mathrm{c}}(H) = \bar{\sigma}/(2\mu_0 H M_s) \quad \text{and} \tag{1a}$$

$$\mathcal{P}_{\mathrm{c}}(H) = \rho_{\mathrm{DW}}^{\mathrm{meta}}(H)[1 - \zeta(H)/\sqrt{1+\zeta^2(H)}], \tag{1b}$$

where $\bar{\sigma}$ is the averaged domain wall energy along the diameter of the half reversed nanodisk and $\zeta(H) = \rho_{\mathrm{DW}}^{\mathrm{meta}}(H)/\mathcal{C}_{\mathrm{c}}(H)$.

The magnetic field dependence of these two critical parameters is shown in Figs. 6(a) and 6(b), respectively. The critical curvature is similar to the domain wall curvature obtained in the case of the infinite 2D-Ising thin film which diverges in a zero field.[27] Unlike the case of droplet nucleation in infinite thin films assumed in Ref. 26, we find analytically that, even in a zero applied magnetic field, the critical volume of the droplet is finite due to the finite value of $\mathcal{L}_{\mathrm{c}}$. In the

nanodisk, in a zero applied magnetic field, the saddle point is reached once the droplet has filled half of the nanodisk with a straight domain wall at the nanodisk diameter position. This corresponds to a critical penetration equal to the radius of the nanodisk [see Fig. 6(c)]. In a finite field, the saddle point is reached before the magnetization reversal of half of the nanodisk, the confined droplet having always a finite curvature. When the applied magnetic field is increased, the critical droplet volume decreases with both $\mathcal{C}_c(H)$ and $\mathcal{P}_c(H)$ decreasing [see Figs. 6(a) and 6(b)].

The activation barrier of the confined 2D-Ising droplet is then given by the energy difference between the configuration of the droplet with the critical situation and the initial configuration with the metastable circular domain wall:

$$\Delta E_{\mathrm{drop}}(H) = 2\rho_{\mathrm{DW}}^{\mathrm{meta}}(H)d\bar{\sigma}(H)\left[\frac{1}{2} - \frac{\zeta(H)}{2}\arccos\left(\frac{\zeta(H)}{\sqrt{1+\zeta(H)^2}}\right) + \frac{1}{2\zeta(H)}\arccos\left(\frac{1}{\sqrt{1+\zeta(H)^2}}\right)\right]$$
$$- 2\rho_{\mathrm{DW}}^{\mathrm{meta}}(H)d\sigma\left(\rho_{\mathrm{DW}}^{\mathrm{meta}}\right)\arccos\left(\frac{\rho_{\mathrm{DW}}^{\mathrm{meta}}(H) - \mathcal{P}_c(H)}{\rho_{\mathrm{DW}}^{\mathrm{meta}}(H)}\right). \quad (2)$$

Unlike in an infinite thin film where the activation energy of a single droplet diverges at a zero field, the activation of the confined droplet is finite and is simply given by the energy cost of the domain wall at the center of the nanodisk: $\Delta E_{\mathrm{drop}}(H=0) = 2\bar{\sigma}R_e d = 1.06\,\mathrm{eV}$. This activation energy, decreasing with magnetic field due to the smaller critical size of the droplet, is plotted in Fig. 4 superimposed with the experimental data. No free parameter is used in this modeling, since the calculated activation energy depends only on the independently determined M_s, K, and A, and the confined droplet growth mechanism provides energy barriers in good agreement with our experimental finding and gives a clear physical mechanism responsible for the low activation energy reported in this paper. This reversal mode does not require modeling of any additional and uncharacterized defects favoring nucleation, as it is controlled by the soft ring state completely determined by the 2D-Ising model above, and is the reason for the rather uniform switching properties of the nanodisk array.

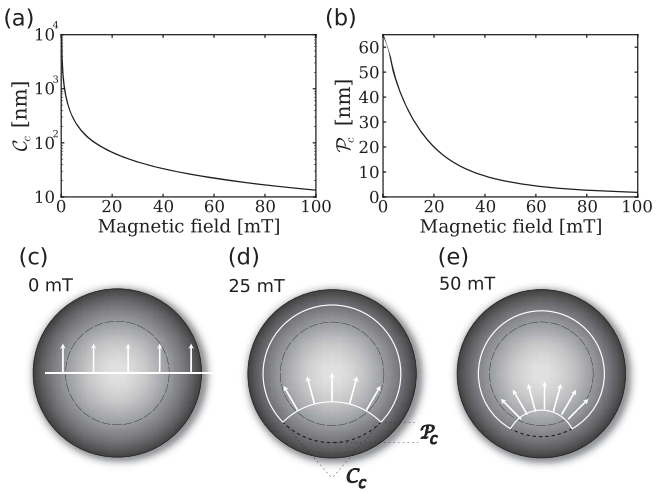

FIG. 6. (a) Evolution of the critical curvature of a single confined droplet versus the applied magnetic field. (b) Evolution of the critical penetration of a single confined droplet in the nanodisk versus the applied magnetic field. (c), (d), and (e) are representations of the micromagnetic state, determined by the white lines representing the positions of the initial metastable domain wall and of the critical droplet under the same applied magnetic fields as in Figs. 5(b), 5(d), and 5(f), respectively. The white arrows represent the direction of the droplet motion.

V. CONCLUSION

Using state-of-the-art *e*-beam lithography and soft He^+ irradiation magnetic patterning techniques, we have fabricated an array of ultrathin Pt/Co(0.5 nm)/Pt nanodisks with perpendicular magnetic anisotropy that allows us to uniquely determine the magnetization reversal mechanism. We show that thermal activation properties cannot be interpreted within the coherent reversal model, nor via the usual random nucleation/domain wall propagation mechanisms. In contrast to previous experiments, the mechanism involved in our nanodisks does not require a nucleation process on extrinsic defects. Reversal is only due to expansion of a magnetic droplet from a metastable circular domain wall stabilized, due to the gradient in the magnetic properties induced by the He^+ irradiation in the outer ring of the irradiated nanodisk. This He^+ irradiation also induces a smoothening of the magnetic properties, and since the droplet growth mechanism is only governed by domain wall propagation, we determine narrow energy barrier and switching field distributions. This process does not contribute to the magnetization stabilization in nanoelements, since it involves a lower activation energy than coherent magnetization reversal, but it does lead to low switching fields H_{SW} even at high frequency. The limitation encountered by the irradiation mask design may be circumvented by the use of Ga^+ focused ion beam (Ref. 30) or the recently demonstrated He^+ ion nanopatterning.[31] For recently proposed hybrid soft/hard layer structures or hybrid nanoparticles,[32] the $H_{\mathrm{SW}}/\Delta E$ ratio can be improved as compared to other nanoparticle based systems proposed for magnetic recording. Finally, the narrow distribution of switching fields in such nanodisk arrays is a vital advantage for their possible use in future magnetic media.

ACKNOWLEDGMENT

This work has been partly supported by the C-Nano French research program (ST-CALIB project).

APPENDIX: MICROMAGNETIC SIMULATIONS

In the main part of this paper, we focused on experimental results and on an analytical modeling of the magnetization reversal. While a full and detailed micromagnetic simulation study is beyond the scope of this paper, we briefly report in this Appendix micromagnetic simulations that confirm the above presented model.

The micromagnetic simulations have been performed using the finite difference OOMMF code.[33] The mesh size used had a lateral size of 1 nm and a thickness of 0.5 nm. In the hard core region, we used the values given in the text above. In order to fit as closely as possible to the magnetic properties of the nanodisk, we also included the exponential variation of M_s, K, and A along the radial distance in the outer irradiated ring (Fig. 1).

In a zero applied magnetic field, the remnant magnetic configuration is a homogeneous state with all moments pointing perpendicular to the nanodisk plane. When increasing the magnetic field, in the direction opposed to the remnant magnetization, a progressive canting of the moments at the periphery of the nanodisk is observed. For a magnetic field larger than 16 mT, this results in a circular domain wall stabilized in the outer irradiated ring [see Fig. 7(a)]. Turning the applied magnetic field back to zero results in the expulsion of the domain wall toward the periphery of the nanodisk. This qualitatively confirms the analytical 2D-Ising model proposed above. A comparison between the field dependence of the existence and of the position of the metastable circular domain wall deduced from the analytical model and from the micromagnetic simulations is shown in Fig. 7(b). In order to derive from the analytical model the position of the metastable circular domain wall position, we made the hypotheses of an Ising spin system and, implicitly, of a zero domain wall width. These two assumptions are the main reasons for the difference between the values derived from the analytical model and from micromagnetic simulations.

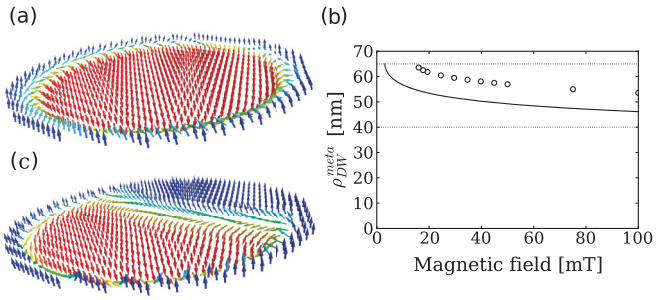

FIG. 7. (Color online) (a) Micromagnetic simulation under an applied magnetic field of 20 mT with a stabilized circular domain wall at $\rho_{DW} = 61.5$ nm. (b) Evolution of the metastable domain wall position as a function of the applied magnetic field. The continuous line corresponds to the analytic model and the open dots to the micromagnetic simulations. (c) Snapshot of the reversed state under $\mu_0 H = 20$ mT starting from the micromagnetic configuration shown in (a) with a manually added slight deformation.

At 0 K, a droplet such as the one proposed as the responsible mechanism for the magnetization reversal of the nanodisk cannot be obtained from micromagnetic simulations. Therefore, starting from the metastable circular domain wall as the initial state, we manually reversed the magnetization in a small volume of the nanodisk in order to drive such a thermally activated magnetization reversal mechanism. This volume was a half disk whose center is located on the metastable circular domain wall, and with a typical radius of a few nanometers. Applying a magnetic field results in the expansion of the reversed magnetization by the motion of the domain wall from this deformation as depicted in the droplet model [see Fig. 7(c)] with a slight displacement, ∼1 nm, of the circular domain wall toward the inner core.

*jean-paul.adam@u-psud.fr
†Present address: Institut d'Électronique Fondamentale, Univ Paris-Sud, CNRS UMR 8622, F-91405 Orsay cedex, France.

[1] E. C. Stoner and E. P. Wohlfarth, Philos. Trans. R. Soc. London A **240**, 599 (1948).
[2] L. Néel, Ann. Geophys. **5**, 99 (1949).
[3] W. F. Brown Jr., Phys. Rev. **130**, 1677 (1963).
[4] W. F. Brown Jr., Phys. Rev. **105**, 1479 (1957).
[5] A. Aharoni and S. Shtrikman, Phys. Rev. **109**, 1522 (1958).
[6] A. Aharoni, Phys. Rev. **119**, 127 (1960).
[7] D. A. Garanin and H. Kachkachi, Phys. Rev. Lett. **90**, 065504 (2003).
[8] W. C. Uhlig and J. Shi, Appl. Phys. Lett. **84**, 759 (2004).
[9] J. S. Broz, H. B. Braun, O. Brodbeck, W. Baltensperger, and J. S. Helman, Phys. Rev. Lett. **65**, 787 (1990).
[10] H.-B. Braun, Phys. Rev. Lett. **71**, 3557 (1993).
[11] S. Krause, G. Herzog, T. Stapelfeldt, L. Berbil-Bautista, M. Bode, E. Y. Vedmedenko, and R. Wiesendanger, Phys. Rev. Lett. **103**, 127202 (2009).
[12] W. Wernsdorfer, B. Doudin, D. Mailly, K. Hasselbach, A. Benoit, J. Meier, J.-P. Ansermet, and B. Barbara, Phys. Rev. Lett. **77**, 1873 (1996).
[13] J.-P. Jamet, S. Lemerle, P. Meyer, J. Ferré, B. Bartenlian, N. Bardou, C. Chappert, P. Veillet, F. Rousseaux, D. Decanini, and H. Launois, Phys. Rev. B **57**, 14320 (1998).
[14] T. Thomson, G. Hu, and B. D. Terris, Phys. Rev. Lett. **96**, 257204 (2006).
[15] J. Ferré and J.-P. Jamet, in *Handbook of Magnetism and Advanced Magnetic Materials*, edited by H. Kronmüller and S. Parkin (J. Wiley & Sons, Chichester, UK, 2007), Vol. 3, p. 1710.
[16] C. Chappert, H. Bernas, J. Ferré, V. Kottler, J.-P. Jamet, Y. Chen, E. Cambril, T. Devolder, F. Rousseaux, V. Mathet, and H. Launois, Science **280**, 1919 (1998).
[17] H. Bernas, T. Devolder, C. Chappert, J. Ferré, V. Kottler, Y. Chen, C. Vieu, J.-P. Jamet, V. Mathet, E. Cambril, O. Kaitasov, S. Lemerle, F. Rousseaux, and H. Launois, Nucl. Instrum. Methods, Sect. B **148**, 872 (1999).

[18] V. Repain, M. Bauer, J.-P. Jamet, J. Ferré, A. Mougin, C. Chappert, and H. Bernas, Europhys. Lett. **68**, 460 (2004).

[19] T. Devolder, C. Chappert, V. Mathet, H. Bernas, Y. Chen, J.-P. Jamet, and J. Ferré, J. Appl. Phys. **87**, 8671 (2000).

[20] T. Devolder and H. Bernas, in *Materials Science with Ion Beams*, edited by H. Bernas, Topics in Applied Physics Vol. 116 (Springer, Berlin, 2010), p 227.

[21] W. Wernsdorfer, E. B. Orozco, K. Hasselbach, A. Benoit, B. Barbara, N. Demoncy, A. Loiseau, H. Pascard, and D. Mailly, Phys. Rev. Lett. **78**, 1791 (1997).

[22] M. Lederman, S. Schultz, and M. Ozaki, Phys. Rev. Lett. **73**, 1986 (1994).

[23] J.-P. Adam, S. Rohart, J.-P. Jamet, A. Mougin, J. Ferré, H. Bernas, G. Faini, and J. Fassbender, J. Magn. Soc. Jpn. **33**, 498 (2009).

[24] The τ_0 value found from the Néel-Brown model is 10^{-12} s, while the characteristic time of precession in the domain wall is on the order of 10^{-10} s. Therefore we chose $\tau_0 = 10^{-11}$ s to infer energy barriers from our measurements, and the vertical error bars in Fig. 4 represents this uncertainty on τ_0.

[25] J. M. Shaw, S. E. Russek, T. Thomson, M. J. Donahue, B. D. Terris, O. Hellwig, E. Dobisz, and M. L. Schneider, Phys. Rev. B **78**, 024414 (2008).

[26] J. Moritz, B. Dieny, J. P. Nozières, Y. Pennec, J. Camarero, and S. Pizzini, Phys. Rev. B **71**, 100402 (2005).

[27] H. L. Richards, S. W. Sides, M. A. Novotny, and P. A. Rikvold, J. Magn. Magn. Mater. **150**, 37 (1995).

[28] D. Hinzke and U. Nowak, Phys. Rev. B **58**, 265 (1998).

[29] The relevance of this model was again checked by micromagnetic simulations which show that in a given field, a sufficient deformation of the circular domain wall actually induces magnetization reversal of the entire nanodisk (see Appendix and Fig. 7).

[30] J.-P. Adam, J.-P. Jamet, J. Ferré, A. Mougin, S. Rohart, R. Weil, E. Bourhis, and J. Gierak, Nanotechnology **21**, 445302 (2010).

[31] D. C. Bell, M. C. Lemme, L. A. Stern, J. R. Williams, and C. M. Marcus, Nanotechnology **20**, 455301 (2009).

[32] R. H. Victora and X. Shen, IEEE Trans. Magn. **41**, 537 (2005).

[33] The code is available at http://math.nist.gov/oommf.